Remarkably enhanced density and specific activity of active sites in Al-rich Cu-, Fe- and Co-beta zeolites for selective catalytic reduction of NO$_x$

Petr Sazama[*], Radim Pilar, Lukasz Mokrzycki, Alena Vondrova, Dalibor Kaucky, Jan Plsek, Stepan Sklenak, Petr Stastny, Petr Klein

J. Heyrovský Institute of Physical Chemistry, Academy of Sciences of the Czech Republic, Prague, Czech Republic

ARTICLE INFO

ABSTRACT

The efficiency of catalysts for abatement of emissions of nitrogen oxides (NO$_x$) from stationary and especially mobile sources using selective catalytic reduction (SCR) is obviously still not sufficient to meet increasingly more stringent environmental limits. We demonstrate that the conversion of NO$_x$ to nitrogen under the relevant conditions of the SCR-NO$_x$ can be dramatically increased using Al-rich beta zeolite catalysts with a high concentration of transition metal counter-ions, bearing extra-framework oxygen ligand (M/M-oxo, where M = Cu, Co, Fe), particularly in the low-temperature region as well as at high space velocities. The high concentration of framework Al and corresponding high population of AlSiAl sequences in template-free synthesized Al-rich beta zeolite does not result in relative increased binding of bare non-reducible and non-active M(II) ions. To the contrary, the unparalleled high concentration of the atomically dispersed M/M-oxo counter-ions with appropriate redox properties and enhanced specific activities provides 3–12 times higher reaction rates for the SCR-NO$_x$ using ammonia, methane and propane as reducing agents compared to state-of-the-art Si-rich zeolite catalysts.

© 2016 Elsevier B.V. All rights reserved.

1. Introduction

The versatile redox state and open coordination sphere of Fe, Cu and Co ions in the extra-framework sites of structurally stable high-silica zeolites provide high and stable activity in selective catalytic reduction of nitrogen oxides. Fe(II)/Fe(III), Cu(I)/Cu(II), and Co(II)/Co(III) counter-ions facilitate oxidation of NO and selective catalytic reduction of NO$_x$ by ammonia (NH$_3$-SCR-NO$_x$) [1–5] or hydrocarbons (C$_x$H$_y$-SCR-NO$_x$) as reducing agents [6–9]. The negative charge of the zeolite framework originating from the substitution of the framework Si(IV) by Al(III) controls the concentration of the ion-exchanged cations and their electronic properties, i.e. a low and/or versatile redox state depending on the density of the available electrons. An increase in the concentration of Al atoms in the framework of silica-rich zeolites (up to Si/Al ∼ 11) resulted in an increased concentration of the ionic species with a proper redox structure and in increased reaction rates in SCR-NO$_x$ [10,11]. However, a further increase in the Al content attained using faujasite or mordenite zeolites (Si/Al 3–5) resulted in the formation of Al-Si-Al sequences in the zeolite framework, which form the cationic sites for divalent and strongly stabilized barely reducible cations without catalytic activity [10,12,13]. Consequently, the maximum concentration of active centres of appropriate structure and properties relevant for the redox reactions has been limited by the concentration of Al in silica-rich zeolites available. Standard syntheses of the most common ZSM-5 and beta zeolites provide content of the framework Al corresponding Si/Al ≥ 11.

The discovery of new synthesis procedures yielding a high concentration of tetrahedrally coordinated Al in the framework of the beta zeolite from a dense system containing a minimum of template [14,15] or synthesis routes employing seeding of Si-rich beta crystals in the complete absence of an organic structure-directing agent [16–30] led to the synthesis of Al-rich beta zeolites with Si/Al ≥ 4. ^{29}Si MAS NMR studies revealed that Al in Al-rich beta zeolites inevitably forms Al-Si-Al sequences similar to other Al-rich zeolites [23,24,28,30]. However, the Al-Si-Al sequences in Al-rich beta zeolites are mostly located in the zeolite wall separating two channels and the Al atoms of the sequence thus face two channels (see Fig. 1 and Ref. [30]). The negative charge of the framework originating from such sequences cannot be balanced in dehydrated

* Corresponding author.
E-mail address: petr.sazama@jh-inst.cas.cz (P. Sazama).
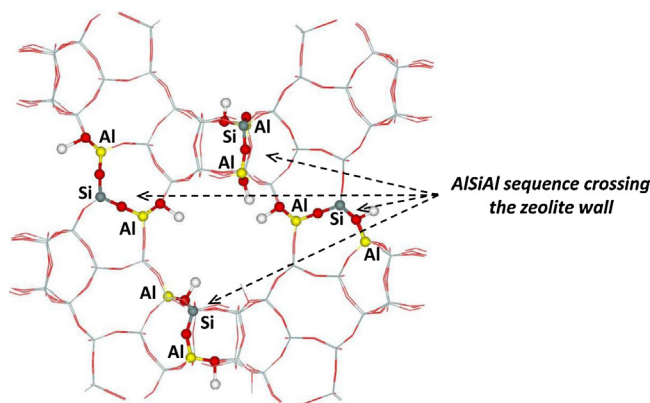
Fig. 1. Illustration of the structure of the Al-rich beta zeolite with the prevailing arrangement of Al atoms in AlSiAl sequences crossing the zeolite walls and forming cationic sites in two different channels. Oxygen and hydrogen in red and white, respectively. (For interpretation of the references to colour in this figure legend, the reader is referred to the web version of this article.)

zeolite by bare divalent cations; instead the charge can be compensated by two formally monovalent metal-oxo species located in different channels. Therefore the high concentration of Al atoms in the framework of Al-rich beta zeolites does not result in relatively increased formation of bare non-reducible and non-active divalent ions but the Al-Si-Al sequences forming the zeolite beta wall provide cationic sites like in a Si-rich zeolite but in significantly increased concentrations [29,30].

This study was performed to illustrate the unparalleled potential of Al-rich beta zeolites for obtaining significantly increased concentrations of active centres with enhanced specific activities for deNO$_x$ reactions. The objective of this paper is not a detailed analysis of the structure of the active sites on a molecular level, but rather to evaluate the effect of Al-rich beta zeolite on the activity of the M/M-oxo counter-ions (M = Cu, Co, Fe). Al-rich *BEA with Cu, Co and Fe sites were prepared as they are among the most active for SCR-NO using ammonia, methane and propane, respectively, and their activities were quantitatively compared with state-of-the-art Si-rich *BEA zeolites. The increased concentration and specific activities of active centres can clearly contribute to an improvement in the efficiency of SCR-NO$_x$.

2. Experimental

2.1. Parent zeolites and preparation of Cu-, Fe- and Co-*BEA catalysts

Al-rich beta zeolites were hydrothermally synthesized from aluminosilicate synthesis gel prepared from NaAlO$_2$ and fumed silica (Cabosil) in the absence of an organic structure-directing agent and using seeding of calcined beta crystals. Details of the procedure were reported previously [28]. The zeolite products have molar Si/Al ratios of 4.2 and 4.6 and were denoted as *BEA/4 and *BEA/5. The high-silica beta zeolites kindly supplied by the Tricat Company (now part of Clariant), (Si/Al 11.5, TZB-212) and Zeolyst International (CP814B-25, Si/Al 12.5), denoted as *BEA/11 and *BEA/12, respectively, were used for preparation of Cu-, Fe- and Co-beta catalysts used as a standards for comparing the catalytic properties. *BEA/4 and *BEA/5 consist of well-developed crystals ~0.4 μm in size with a high surface area of 510 and 482 mg^{-1}, respectively (Table 1). *BEA/11 and *BEA/12 consisted of very small crystallites ~0.05 and ~0.1 μm in size, respectively, and exhibited high surface areas of 617 and 605 m^2 g^{-1}, respectively. The intensities and patterns of the X-ray diffraction lines for all the beta zeolites are characteristic for the well-developed crystalline structure of *BEA topology (Supplement 1). The ^{29}Si MAS NMR spectra yielded

Table 1
Characteristics of parent zeolites.

Sample	Si/Al[a]	Si/Al$_{FR}$[b]	c_{Al}[a]	Crystal size	S
			mol g^{-1}	μm	m^2 g^{-1}
*BEA/4	4.2	4.7	3.1	~0.4	510
*BEA/5	4.6	4.8	3.0	~0.4	482
*BEA/11	11.3	11.5	1.4	~0.05	617
*BEA/12	12.5	13	1.2	~0.1	605

[a] From chemical analysis of the Na$^+$ form of zeolites.
[b] From ^{29}Si MAS NMR spectra of the Na$^+$ form of zeolites.

framework Si/Al$_{FR}$ ratios comparable with those obtained from the chemical analysis (Table 1).

Fe-*BEA were prepared by ion exchange of the respective *BEA zeolites with aqueous FeSO$_4$ solution under nitrogen atmosphere at 95 °C for 14 h as described in Ref. [28]. Cu- and Co-*BEA were prepared by triply repeated ion exchange with 100 ml of 0.05 M Cu(NO$_3$)$_2$ and Co(NO$_3$)$_2$ solutions, respectively, per gram of zeolite at RT for 24 h. The obtained materials were thoroughly washed with demineralized water and dried in the open air.

2.2. Structural analysis

X-ray powder diffraction (XRD) patterns were obtained using a Bruker AXSD8 Advance diffractometer with a graphite monochromator, a position sensitive detector (Våntec-1) and CuKα radiation in Bragg–Brentano geometry. The chemical compositions of the parent and prepared Cu-, Fe- and Co-beta zeolites were determined by X-ray fluorescence spectroscopy using a PW 1404 (Philips). The UV–vis–NIR reflectance spectra of Cu-, Fe- and Co-beta zeolites were recorded on a Perkin–Elmer Lambda 950 UV–vis–NIR spectrometer equipped with an integrating sphere for diffuse reflectance measurements covered with Spectralon. The Schuster–Kubelka–Munk function F(R$_\infty$) = (1 − R$_\infty$)^2/2R$_\infty$, where R$_\infty$ is the diffuse reflectance from a semi-infinite layer, was used for recalculation of the reflectances to F(R$_\infty$) proportional to the absorption coefficient. The XPS measurements of Co-*BEA zeolites pre-treated at 400 °C in a flow of synthetic air for 30 min were performed in a VG ESCA3 MkII electron spectrometer with a base pressure <10^{-9} mbar. AlKα radiation was used for excitation of the electrons. The energy of electrons was analysed using a hemispherical analyser operating at a constant pass energy of 50 eV. The spectra were calibrated by setting the C1s peak belonging to adventitious carbon on the sample surface at the binding energy of 284.8 eV.

Table 2
Composition of Cu-*BEA, and reaction rate r and TOF for SCR-NO$_x$ using propane or ammonia as reducing agents.

Sample	C_{Cu} wt.%	Cu/Al	C$_3$H$_8$-SCR-NO				NH$_3$-SCR-NO			
			350 °C		375 °C		208 °C		258 °C	
			r^a mol$_{NO}$ kg^{-1} h^{-1}	TOF^b h^{-1}	r^a mol$_{NO}$ kg^{-1} h^{-1}	TOF^b h^{-1}	r^a mol$_{NO}$ kg^{-1} h^{-1}	TOF^b h^{-1}	r^a mol$_{NO}$ kg^{-1} h^{-1}	TOF^b h^{-1}
Cu-*BEA/4	6.8	0.78	2.24	2.10	3.82	3.57	47.1	44.1	91.0	85.2
Cu-*BEA/12	3.0	0.86	0.66	1.38	1.05	2.20	5.7	12.0	12.1	25.3

[a] Reaction rate calculated from the first-order kinetics.
[b] TOF (mol$_{NO}$ mol$_{Cu}^{-1}$ h^{-1}).

Table 3
Composition of Fe-*BEA, and TOF and reaction rate r for C$_3$H$_8$-SCR-NO$_x$.

Sample	c_{Fe} wt.%	Fe/Al	275 °C		300 °C	
			r^a mol$_{NO}$ kg^{-1} h^{-1}	TOF^b h^{-1}	r^a mol$_{NO}$ kg^{-1} h^{-1}	TOF^b h^{-1}
Fe-*BEA/5	11.7	0.73	2.0	1.0	4.5	2.1
Fe-*BEA/11	5.3	0.77	0.7	0.7	1.5	1.5

[a] Reaction rate calculated from the first-order kinetics.
[b] TOF (mol$_{NO}$ mol$_{Fe}^{-1}$ h^{-1}).

Table 4
Composition of Co-*BEA, and TOF and reaction rate r for CH$_4$-SCR-NO$_x$.

Sample	c_{Co} wt.%	Co/Al	425 °C			450 °C		
			x_{NOx} %	r^a mol$_{NO}$ kg^{-1} h^{-1}	TOF^b h^{-1}	x_{NOx} %	r^a mol$_{NO}$ kg^{-1} h^{-1}	TOF^b h^{-1}
Co-*BEA/4	8.8	0.53	25.1	2.3	1.54	33.5	3.2	2.2
Co-*BEA/12	2.6	0.37	2.1	0.17	0.38	3.3	0.26	0.60

[a] Reaction rate calculated from the first-order kinetics.
[b] TOF (mol$_{NO}$ mol$_{Co}^{-1}$ h^{-1}).

2.3. Kinetic analysis

NH$_3$-SCR-NO$_x$ was performed in a quartz tubular down-flow reactor with a micro thermocouple placed in the centre of the catalyst bed and by using the reactant gases (NO, NH$_3$, and O$_2$) and the carrier gas (He) fed from independent mass flow controllers. The concentrations of reactants and products were analysed stepwise at steady-state at temperatures from 500 to 200 °C using an UV photometric analyser (ABB AO2000-Limas11UV) for NO, NO$_2$ and NH$_3$ and an infrared absorption photometer (ABB Uras26 EL3020) for N$_2$O. Typically, the temperature was kept constant for 2 h for each temperature step. The experimental conditions for the SCR reaction were as follows: total gas flow rate 350 cm^3 min^{-1} and catalyst weight 5 mg corresponding GHSV 2,100,000 h^{-1}; NO 450 ppm; NH$_3$ 470 ppm; O$_2$ 2%; balance He. NO$_x$ conversion was defined as the reduction of NO and NO$_2$ to N$_2$ and N$_2$O. The reproducibility of NO$_x$ conversion was ±2%. A kinetic regime under the reaction conditions was confirmed by a variation in the total gas flow and weight of catalyst. Small crystallites of used *BEA zeolites (~0.05–0.4 μm) guaranteed the absence of intra-crystalline diffusion constraints to the overall reaction rates for the flow rates and temperatures <450 °C (cf. the conditions given in Refs. [4,31]). The reaction rates of the NO$_x$ to N$_2$ conversion were calculated using a pseudo-first-order kinetic equation written as r = F/W*(−ln(1−x)), where x is the conversion, F is the flow rate of the feed (mol of NO per h^{-1}), and W is the weight of the catalyst (kg), in agreement with the first reaction order with respect to NO [32]. Ammonia as well as water exhibit zero order kinetics [32,33] and changes in the oxygen concentration do not significantly affect the reaction rate, as it is present in a high excess. The TOF values were calculated for the reactions per total Cu (mol$_{NOx}$ mol$_{Cu}^{-1}$ s^{-1}).

A fixed-bed quartz tubular down-flow reactor with 100 mg of a catalyst in the form of 0.2–0.4 mm grains was used to investigate the catalyst activity in SCR-NO$_x$ using propane and methane. A reactant mixture consisting of 1000 ppm NO, 1000 ppm C$_3$H$_8$ or

3000 ppm CH$_4$, 3% O$_2$ and 1% H$_2$O in He as a balance was kept at a total flow rate of 300 ml min^{-1} corresponding to GHSV 90,000 h^{-1}. The concentrations of NO$_x$ (NO, NO$_2$) and N$_2$O at the inlet and outlet of the reactor were continuously monitored by an NO/NO$_x$ chemiluminescence analyser (API MLU 200AH) and IR analyser (ABB Advance Optima Uras 14), respectively, and recorded stepwise under steady state reaction conditions for each temperature. An on-line-connected Hewlett Packard 6090 gas chromatograph was used for analysis of the concentrations of C$_1$–C$_3$ hydrocarbons, O$_2$, N$_2$, N$_2$O, CO, and CO$_2$. Two gaseous samples were simultaneously injected through 10-port valves into two branches of the gas chromatograph equipped with a thermal conductivity detector (TCD) for analysis of O$_2$, N$_2$, N$_2$O, CO, and CO$_2$, and a flame ionization detector (FID) for analysis of C$_1$-C$_3$ hydrocarbons (for more details see Ref. [34]). The influence of external mass and heat transfer on the SCR reaction was excluded by experiments with variations in the catalyst weights and flow rates at constant GHSV. The catalytic tests were repeated twice, and the reproducibility in NO$_x$ conversion was ±1%. The rates of the NO$_x$ reaction (r_{SCR}) per gram of catalyst (mol g^{-1} s^{-1}) were calculated using the assumption of pseudo-first-order kinetics. Only CH$_4$ and C$_3$H$_8$ conversion values <30% were considered. Changes in the oxygen and water concentrations resulting from the reaction do not affect the reaction rate, as they are present in a high excess. The turn-over-frequencies (TOF) were expressed per total content of metal (M = Cu, Co, Fe), (mol$_{NO}$ mol$_M^{-1}$ s^{-1}). The apparent activation energies and preexponential factors were estimated from the Arrhenius plots.

3. Results and discussions

3.1. Selective catalytic reduction of NO over Cu-*BEA zeolites

3.1.1. Structure of Cu sites

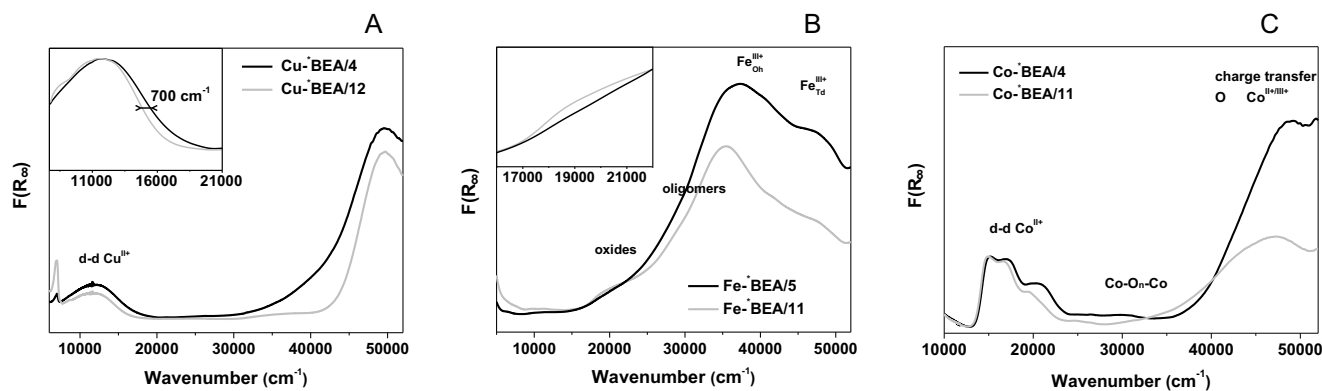A comparative study of Cu-ZSM-5 and Cu-*BEA zeolites performed by Corma et al. [35] showed that Cu-*BEA zeolites are

Fig. 2. DR UV–vis–NIR spectra of hydrated (A) Cu-*BEA, (B) Fe-*BEA and dehydrated (C) Co-*BEA Al-rich and Si-rich zeolites.

stable SCR catalysts yielding activities as high as those of Cu-ZSM-5 described by Iwamoto and Hamada [36]. The maximum activity for Cu-*BEA zeolites were found in preceding studies for an overexchanged samples at exchange levels of about 150% with Cu in the cationic forms [37]. Therefore, to analyse the potential of Al-rich *BEA zeolite for the preparation of a functional catalysts for SCR reactions, a sample of Al-rich Cu-*BEA (Si/Al = 4.2) was prepared with a copper loading corresponding to Cu/Al 0.78 and compared with Si-rich Cu-*BEA (Si/Al = 12.6, Cu/Al = 0.86), (Table 2). The UV–vis–NIR diffuse reflectance spectra of the as-prepared Cu-*BEA samples are shown in Fig. 2A. Intense absorption bands were found at 12,000 cm^{-1} due to Cu(II) in an octahedral environment [38] and above 40,000 cm^{-1} due to the Cu → O charge-transition (CT). The significantly higher intensity of the d–d absorption band of Cu(II) for Al-rich compared to Si-rich Cu-*BEA is proportional to the content of Cu (Table 2). The presence of the band at 12,000 cm^{-1}, and the absence of both an absorption edge characteristic of CuO or Cu$_2$O oxides [38,39] and an adsorption band about 22,000 cm^{-1}

characteristic of (Cu—O—Cu)$^{2+}$ or bis(μ-oxo) dicopper species [7,40] indicate the prevailing presence of isolated Cu^{2+} for both Cu-*BEA samples. The inset in Fig. 2A shows a detail of the bands of d–d transition of Cu^{2+} after normalization. It clearly shows a shift of the high-energy edge of the absorption band to a higher frequency. The shift reflects the replacement of one or more water molecules in octahedrally coordinated the Cu^{2+} hexa-aquocomplex by another ligand, such as the OH group [39]. Thus, the shifts in the absorption band indicate increased relative concentration of monovalent [Cu^{2+}(H$_2$O)$_5$OH$^-$]$^+$ complexes in Cu-*BEA/4 compared to Cu-*BEA/12. The formation of these complexes was found in zeolites with distant single Al atoms bound in different rings of the zeolite framework, able to balance only monovalent cation complexes [39,41,42]. The [Cu^{2+}(H$_2$O)$_5$OH$^-$]$^+$ complexes in Al-rich Cu-*BEA/4 could be located in the vicinity of one of the framework aluminium atoms from the Al-Si-Al sequence crossing the zeolite beta wall and facing two different channels (for illustration see Fig. 3A).
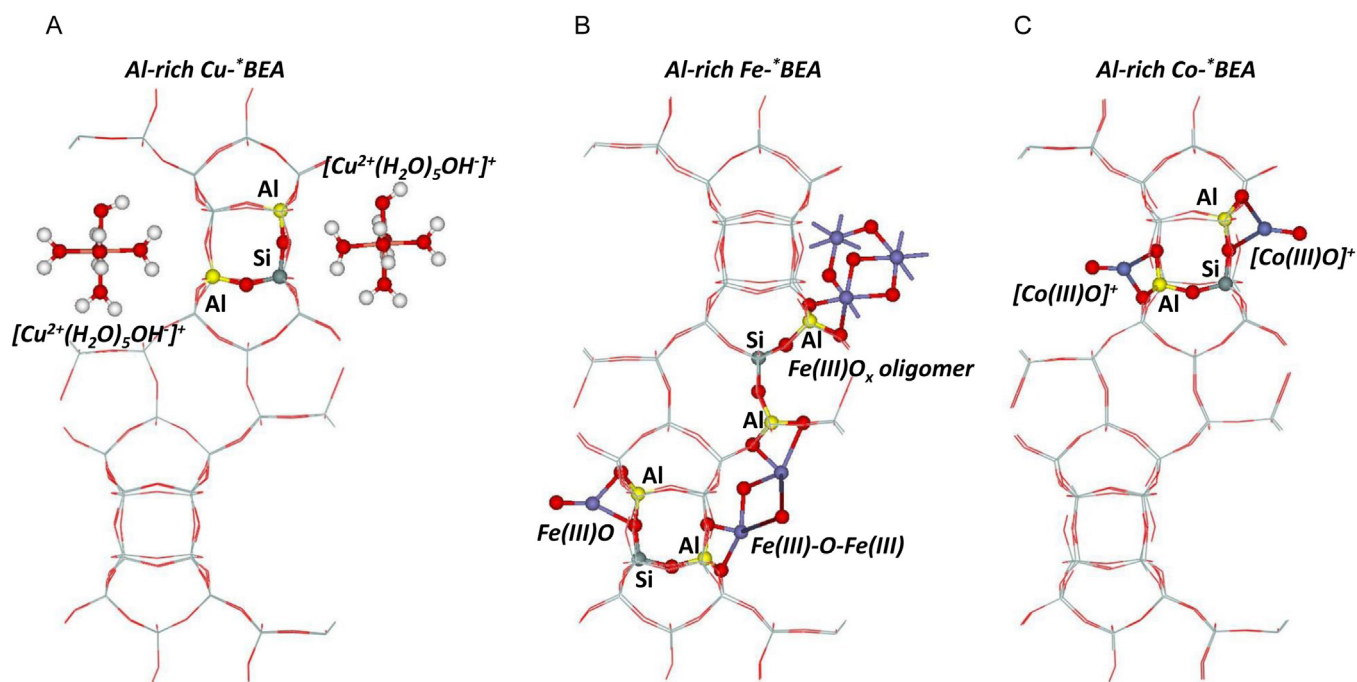

Fig. 3. Illustration of main Cu-, Fe- and Co-species present in Al-rich beta zeolites. (A) Hydrated Al-rich Cu-*BEA, (B) dehydrated Al-rich Fe-*BEA and (C) dehydrated Al-rich Co-*BEA. Oxygens and hydrogens in red and white, respectively. (For interpretation of the references to colour in this figure legend, the reader is referred to the web version of this article.)

3.1.2. Selective catalytic reduction of NO by propane and ammonia

Fig. 4 shows the results obtained for the conversion of NO and C_3H_8, and yields of CO_2, CO and N_2O as a function of temperature for SCR-NO using C_3H_8 as the reducing agent over Si- and Al-rich Cu-*BEA. The Al-rich Cu-*BEA/4 yields significantly higher NO conversions compared to Cu-*BEA/12; note that the measurements were performed at high GHSV of 90,000 h^{-1} and in the presence of water vapour. The NO and C_3H_8 conversions began at 300 °C and increased with increasing reaction temperature maintaining efficient utilization of propane in the whole temperature region. The SCR reaction is highly selective for N_2 and CO_2 whereas N_2O and CO were detected in the products with yields below 2%. Stable values of NO_x and propane conversions and N_2O and CO yields as a function of time-on-stream were obtained in the presence of water vapour at 400 °C for 48 h. This indicates sufficient structural stability of Al-rich Cu-*BEA for the temperatures and water vapour concentrations typical of stationary deNO$_x$ units. The Arrhenius plots yield linear dependences with apparent activation energies (E_a) higher for Al-rich Cu-*BEA/4 but compensated by a several-order-of-magnitude higher pre-exponential factor compensating E_a. The reaction rates of NO_x conversion and turn-over-frequency values per total Cu (TOF_{Cu}) are listed in Table 2. The reaction rates at 350 and 375 °C for Al-rich Cu-*BEA/4 are ca 3.5 times higher, and TOF_{Cu} are ca 1.5 times higher than those over Si-rich Cu-*BEA/12. More than twice the concentration of isolated cationic Cu species in Al-rich Cu-*BEA/4 and higher specific activity of these sites result in a catalytic performance of Cu-*BEA/4 which significantly outperforms the Si-rich analogue.

Conversions of NO_x and NH_3 in NH_3-SCR-NO_x and yield of N_2O as a function of temperature are compared for Al-rich and Si-rich Cu-*BEA zeolites in Fig. 5. The Al-rich Cu-*BEA/4 catalyst provided dramatically increased NO conversions in the low-temperature region as previously reported by Xu et al. [43]. The Si-rich Cu-*BEA/12 gives a NO conversion of 8% at an initial temperature of 208 °C, whereas the Cu-*BEA/4 sample yields 42% conversion at the same temperature. From the conversions in Fig. 5, specific integral reaction rates were calculated and are given in Table 2. These rates at 208 and 258 °C were, respectively, 47.1 and 91.0 of converted NO per kg catalyst and hour for Cu-*BEA/4 and 5.7 and 12.1 of converted NO per kg catalyst and hour for Cu-*BEA/12. Thus the reaction rates were ca 8 times higher over the Al-rich Cu-*BEA/4 zeolite. The remarkable improvement in the catalytic performance reflected in the lower apparent activation energy and higher pre-exponential factor for Al-rich Cu-*BEA is in accordance with both the higher concentration of active sites and their higher specific activity. Both Cu-*BEA samples yielded a low amount of N_2O in the low temperature region ($\leq$5%) but the production become substantial at temperatures above 350 °C, probably due to non-selective conversion of ammonia.

There is a consensus in the literature that the Cu sites responsible for the activity in SCR-NO_x by hydrocarbons or ammonia are ion-exchanged Cu species [8,37,44] while clustered Cu species have been connected with non-selective reactions and the formation of undesirable N_2O [45]. The most active sites for the C_3H_8-SCR-NO reaction were suggested, on the bases of the results of complex spectral studies, to be isolated Cu ions with the ability of fast conversion between Cu(II) and Cu(I) [8]. The extraordinary performance of Al-rich Cu-*BEA thus is rationalised by the very high concentration of isolated Cu(II) ions present in hydrated zeolite in the form of monovalent $[Cu(II)(H_2O)_5OH^-]^+$ complexes compensated by the charge from one aluminium atom from the Al-Si-Al sequence crossing the zeolite beta wall. The higher TOF per Cu for the Al-rich Cu-*BEA could indicate either higher activity of the Cu species formed after dehydration from monovalent $[Cu(II)(H_2O)_5OH^-]^+$ complexes compared to $[Cu(II)(H_2O)_6]^{2+}$ or by a synergistic effect caused by the high concentration and close proximity of the isolated Cu ions.

## 3.2. Selective catalytic reduction of NO over Fe-*BEA zeolites

3.2.1. Structure of Fe sites

The UV–vis–NIR spectra of the Al- and Si-rich Fe-*BEA zeolites with comparable Fe/Al ratios of 0.77 and 0.73, respectively, are compared in Fig. 2B. Spectra of both Fe-*BEA zeolites are characterised by a low intensity absorption edge at 18,000 cm^{-1} reflecting a low concentration of small Fe oxide particles [4,31,46], a band at 29,000 cm^{-1} attributed to polynuclear Fe(III)-oxo complexes [4,31,47,48], and the broad absorptions with maxima at 39,000 and 47,000 cm^{-1} connected with dinuclear or isolated Fe(III)-oxo species with T_d and O_h coordination [4,31,49]. With Al-rich Fe-*BEA/5, the overall intensity of the CT absorptions with maxima at 29,000, 39,000 and 47,000 cm^{-1} is significantly increased and the adsorption at 18,000 cm^{-1} reduced compared to the Si-rich Fe-*BEA/11. This indicates that the high density of the framework charge of Al-rich *BEA facilitates the formation of significantly higher amount of highly dispersed Fe(III)-oxo cations and hinders the formation of Fe-oxides at comparable Fe/Al ratios. For illustration of Fe species in Al-rich Fe-*BEA see Fig. 3B.

3.2.2. Selective catalytic reduction of NO by C_3H_8

Fig. 6 depicts the conversions of NO and C_3H_8, and yields of N_2O, CO and CO_2 as a function of temperature in C_3H_8-SCR-NO over the Si- and Al-rich Fe-*BEA zeolites. With Si-rich Fe-*BEA/11 the conversion first started to increase at a temperature of ca. 250 °C and reached a maximum of 30% at ca. 350 °C before declining again. However, when Al-rich Fe-*BEA/5 was used, NO_x reduction started at 225 °C and reached a maximum of 52% at 325 °C. Thus the use of Al-rich *BEA for preparation of the Fe-catalyst had a positive effect on NO_x reduction in the whole temperature region, although this is not as dramatic as when using the Cu-*BEA catalyst. Fe-*BEA catalysts are also less selective than Cu-*BEA; with Al-rich Fe-*BEA, the yield of CO and N_2O began to increase at a temperature of around 250 °C and reached a maximum of 30 and 3 ppm, respectively, at around 300 °C. The similar apparent activation energies and the higher pre-exponential factor estimated from the Arrhenius plots for Fe-*BEA/5 are consistent with higher concentrations of Fe(III) cations as the active sites. The slightly higher TOF and significantly enhanced concentration of Fe(III) ions resulted in a three times higher reaction rate (Table 3).

Previously we reported the dramatic enhancement of SCR-NO_x over Al-rich Fe-*BEA catalyst using ammonia as a reducing agent and higher hydrothermal stability compared to a Si-rich Fe-*BEA [28]. The reduction of NO_x to molecular nitrogen using hydrocarbons instead of ammonia would be the preferred route [50,51], but the activity of current catalysts is insufficient for practical applications. The capacity of high-silica zeolites for the formation and stabilization of isolated bare Fe ions or dinuclear Fe(III)-oxo species in cationic sites, suggested as the most active sites for C_3H_8-SCR-NO [51,52], was limited by the low concentration of appropriately distributed Al in the zeolite framework. The presence of framework Al atoms corresponding to molar Si/Al ratio ~4 and the charge from a Al-Si-Al sequence distributed into different channels result in the formation of the extraordinarily high concentration of cationic sites and enables partial compensation of the positive charge (Fe/Al 0.73) of the large number of isolated or dimeric Fe(III)-oxo species at Fe loading as high as 11.7 wt.%. The partial compensation of the positive charge of Fe(III)-oxo species by the local negative charge originating from Al-Si-Al sequences separated by the zeolite wall facilitates the redox cycle involving oxygen from the reaction
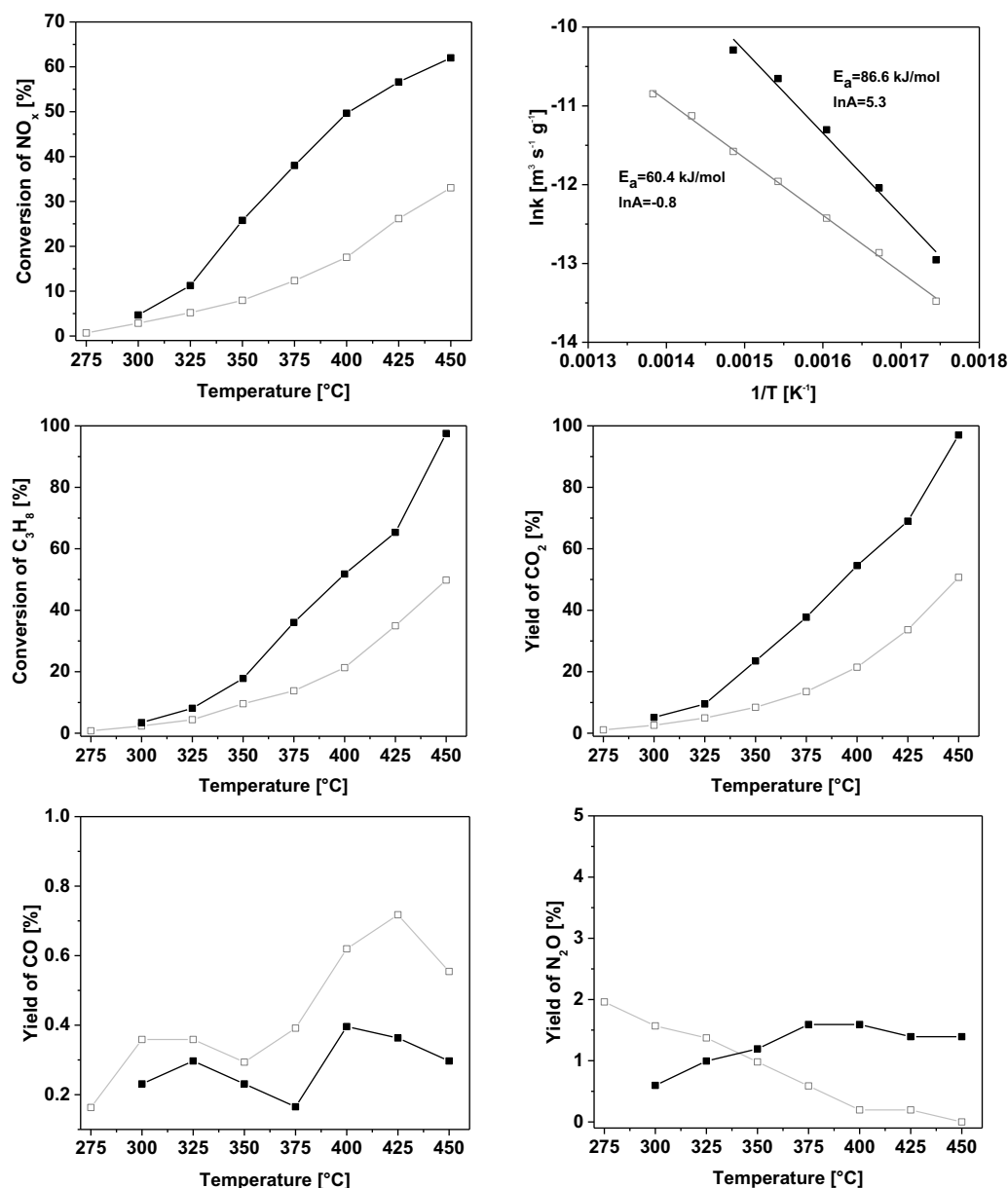
Fig. 4. C_3H_8-SCR-NO over Cu-*BEA/4 (■) and Cu-*BEA/12 (□) catalysts as a function of temperature. Reaction conditions: 1000 ppm NO, 1000 ppm C_3H_8, 2.5% O_2, and 1% H_2O in He, GHSV 90,000 h^{-1}.

stream and high reaction rate in C_3H_8-SCR-NO_x exceeding three times that of the Si-rich Fe-*BEA zeolite.

3.3. Selective catalytic reduction of NO by methane over Co-*BEA zeolites

It is well established that Co-zeolites are among the most active and selective for the selective catalytic reduction of NO_x to N_2 using methane as the most preferred reducing agent for abatement of NO_x emissions for stationary sources. However, one of the drawbacks of these catalysts was their very poor conversions at temperatures below 500 °C. This problem could be overcome only by a remarkable improvement in NO_x reduction in the low temperature range. It is known that the high excess of water vapour in real exhaust gases (10,000–100,000 ppm H_2O vs. ~1000 ppm NO) suppresses the activity of bare Co due to the competitive adsorption of water molecules on these Co ions with Lewis character [6,53]. Therefore,

in the wet NO_x feed only the $[Co(III)O]^+$ oxo-species were found to act as the most active sites [6,53].

3.3.1. Structure of Co sites

Detailed analysis of the structure of the arrangement of cobalt species in Al-rich beta zeolites was described in earlier papers [29,30]. The Al-rich *BEA is able to exchange a large amount of the divalent hexaquo complex $[Co(II)(H_2O)_6]^{2+}$ compensating the negative charge of the framework due to the high population of AlSiAl sequences with AlO_4^- located in one ring, but facing into different channels; for more details, see the illustration in Fig. 1 and Ref. [30]. Following Al-rich Co-*BEA dehydration, the $[Co(II)(H_2O)_6]^{2+}$ complex turns into the $[Co(III)O]^+$ species balancing the charge of one AlO_4^- from the unpaired Al atoms (Fig. 3C). Ion-exchange of Al-rich beta used in this study with cobalt ions yielded a much higher concentration of 8.8 wt.% of cobalt ions compared to 2.6 wt.% for the Si-rich analogue (Table 4). Both as-prepared samples are light pink in colour, typical of the presence of
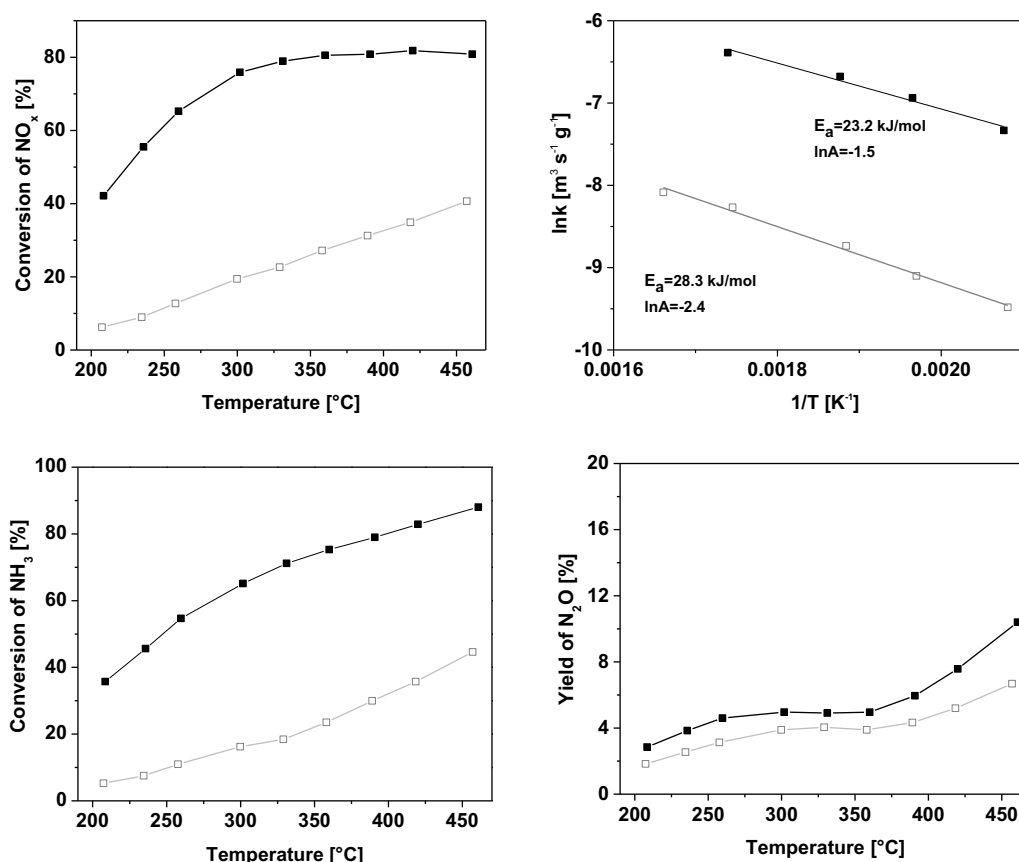
Fig. 5. NH$_3$-SCR-NO over Cu-*BEA/4 (■) and Cu-*BEA/12 (□) catalysts as a function of temperature. Reaction conditions: 450 ppm NO, 470 ppm NH3, 2.5% O$_2$ in He, total flow 350 cm^3 min^{-1} and catalyst weight 5 mg.

octahedral Co(II) hexaquo-complexes. The UV–vis–NIR spectra of the dehydrated Co-*BEA/4 and Co-*BEA/11 (Fig. 2C) showed broad absorption in the region of d–d transitions at 13,000–27,000 cm^{-1} of the high-spin Co(II) ion complexes containing exclusively framework oxygen ligands (bare Co(II) ions), and a very low intensity of absorption of the ligand to metal O → Co(II) charge-transfer of the μ-oxo dinuclear Co species at 28,000–35,000 cm^{-1} [54] and a strong absorption increasing above 40,000 cm^{-1} corresponding to transitions from the framework oxygen atoms to bare Co(II) ions in the cationic sites and also the transitions from extra-framework oxygen(s) to Co ions (Co-oxo species) reaching frequencies well above 50,000 cm^{-1} [30]. The detailed analysis of the d–d transitions of bare Co(II) ions in Al-rich Co-*BEA zeolites (Si/Al 4.5 and 5.1) reported in the preceding paper [30], showed similar relative concentrations of bare Co(II) ions (ranging from 30 to 40% of the total Co), the absence or negligible concentration of the bridged μ-oxo Co(II) complexes, where the rest of the Co (60–70% of total Co) consists in the Co-oxo, [Co(III)O]$^+$ species.

The XPS spectra of the Co2p level for Al- and Si-rich Co-*BEA catalysts calcined in the air at 400 °C followed by evacuation at 350 °C (supplement 2) are characterised by the main peak with maximum at 782.8 eV typical of divalent and trivalent cobalt previously observed for Co$_3$O$_4$ (Co(III) + Co(II)) and CoO (Co(II)) oxides [55–57] or Co(II) and Co(III) ions located in zeolites [58], and a satellite peak at 788 eV characteristic of the Co(II) ions in CoO oxides or zeolites [55,56,58,59]. The nearly identical shape and the maxima of the main and satellite peak of the Co2$p_{2/3}$ line for Al- and Si-rich Co-*BEA indicate the occurrence of cobalt species in very close or identical redox states in both samples. This is in accordance with

the formation of similar Co(II) and [Co(III)O]$^+$ species present only in significantly increased concentrations for Al-rich Co-*BEA.

3.3.2. Selective catalytic reduction of NO by CH$_4$

Conversions of NO$_x$, TOF and reaction rate r for CH$_4$-SCR-NO$_x$ obtained at high GHSV (90,000 h^{-1}) and in the presence of water vapour (1 vol.%) in the reactant stream are compared for the Al- and Si-rich Co-*BEA in Table 4. The high density of active Co-oxo species in Al-rich Co-*BEA/4 facilitates dramatically increased conversion of NO to N$_2$ from 2.1 to 25.1% compared to Co-*BEA/12 at 425 °C. Conversions of NO$_x$ and CH$_4$ and yields of N$_2$O, CO and CO$_2$ as a function of temperature are given in supplement 3. The reaction rates of NO$_x$ conversion and turn-over-frequency values for Al-rich Co-*BEA are twelve and four times higher, respectively, than those over Si-rich Co-*BEA. The extraordinary performance greatly outperforming the Si-rich Co-*BEA sample is suggested to come from the synergistic effect of mutually proximate Co-oxo centres of Al-rich Co-*BEA. The twelve times higher reaction rates per gram of a zeolite and four times higher TOF per Co and per Co-oxo species in Al-rich Co-*BEA/4 are comparable to the improvement obtained in the SCR-NO reaction using propane as a reducing agent reported in the previous study [29].

4. Conclusions

The study of SCR-NO$_x$ using ammonia, methane and propane as reducing agents over Al-rich beta zeolite with the M/M-oxo (M = Cu, Co, Fe) counter-ions showed dramatic increases in the conversion of NO to nitrogen compared to Si-rich beta-zeolite-based catalysts, particularly in the low-temperature region as well as at
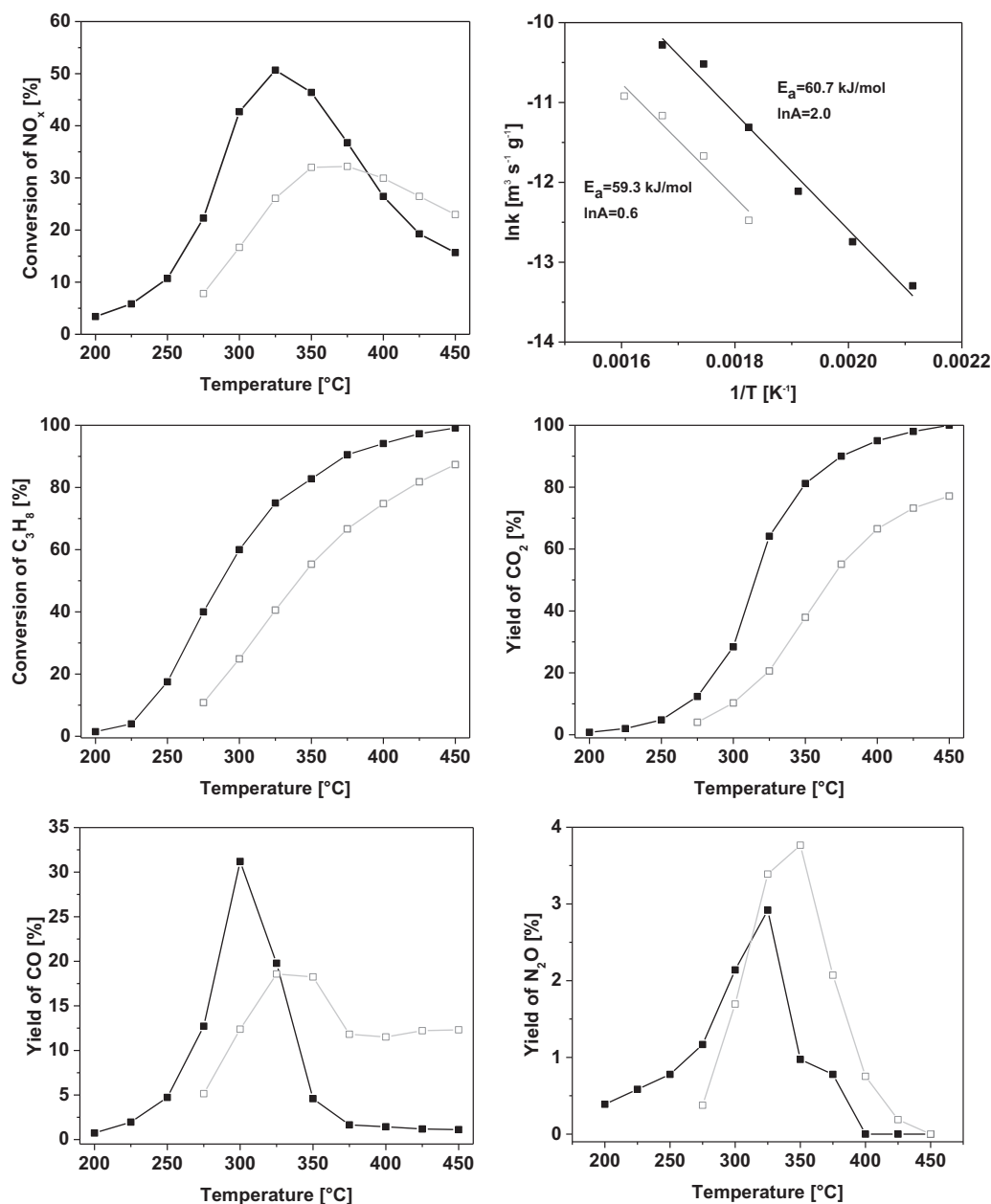
Fig. 6. C$_3$H$_8$-SCR-NO over Fe-*BEA/4 (■) and Fe-*BEA/11 (□) catalysts as a function of temperature. Reaction conditions: 1000 ppm NO, 1000 ppm C$_3$H$_8$, 2.5% O$_2$, and 1% H$_2$O in He, GHSV 90,000 h^{-1}.

high space velocities. Investigation under the relevant conditions of the SCR-NO$_x$ processes in the presence of water vapour in the reaction stream revealed that:

(i) The active Cu centres represented by isolated Cu ions formed after dehydration from monovalent [Cu(II)(H$_2$O)$_5$OH$^-$]$^+$ complexes are populated in a very high concentration in Al-rich Cu-*BEA (Si/Al 4.2, Cu/Al 0.78). The high density and increased specific activity of these atomically dispersed Cu ions lower the activation barrier in the reactions of NH$_3$-SCR-NO$_x$ and C$_3$H$_8$-SCR-NO$_x$ reflected in the 3.5–8 times higher reaction rates compared to the Si-rich Cu-*BEA catalyst.

(ii) Al-rich Fe-*BEA (Fe/Al 0.73, Si/Al 4.2) accommodates a very high concentration of polynuclear Fe(III)-oxo complexes and dinuclear or isolated Fe(III)-oxo species without the formation of significant amounts of Fe-oxides. The unprecedentedly high concentration of highly dispersed Fe(III) ions with appropriate

redox properties for C$_3$H$_8$-SCR-NO yields a three times higher reaction rate compared to Si-rich Fe-*BEA zeolite (Fe/Al 0.77, Si/Al 11.7) and correspondingly increased conversion of NO$_x$ in the whole temperature region.

(iii) The Al-rich Co-*BEA is able to exchange a large amount of a divalent hexaquo complex [Co(II)(H$_2$O)$_6$]$^{2+}$ forming after the dehydration a high concentration of Co-oxo sites highly active for CH$_4$-SCR-NO. Mutually proximate Co-oxo centres in Al-rich Co-*BEA yield twelve times higher reaction rates per gram of zeolite and four times higher TOF per Co.

Acknowledgements

Appendix A. Supplementary data

Supplementary data associated with this article can be found, in the online version, at http://dx.doi.org/10.1016/j.apcatb.2016.02.020.

References

[1] S.M. Maier, A. Jentys, E. Metwalli, P. Muller-Buschbaum, J.A. Lercher, Determination of the redox processes in FeBEA catalysts in NH$_3$-SCR reaction by Mössbauer and X-ray absorption spectroscopy, J. Phys. Chem. Lett. 2 (2011) 950–955.

[2] W.M. Heijboer, A.A. Battiston, A. Knop-Gericke, M. Havecker, H. Bluhm, B.M. Weckhuysen, D.C. Koningsberger, F.M.F. De Groot, Redox behaviour of over-exchanged Fe/ZSM-5 zeolites studied with in-situ soft X-ray absorption spectroscopy, Phys. Chem. Chem. Phys. 5 (2003) 4484–4491.

[3] S.M. Maier, A. Jentys, M. Janousch, J.A. Van Bokhoven, J.A. Lercher, Unique dynamic changes of Fe cationic species under NH$_3$-SCR conditions, J. Phys. Chem. C 116 (2012) 5846–5856.

[4] P. Sazama, N.K. Sathu, E. Tabor, B. Wichterlova, S. Sklenak, Z. Sobalik, Structure and critical function of Fe and acid sites in Fe-ZSM-5 in propane oxidative dehydrogenation with N$_2$O and N$_2$O decomposition, J. Catal. 299 (2013) 188–203.

[5] J. Kim, A. Jentys, S.M. Maier, J.A. Lercher, Characterization of Fe-exchanged BEA zeolite under NH$_3$ selective catalytic reduction conditions, J. Phys. Chem. C 117 (2013) 986–993.

[6] L. Capek, J. Dedecek, P. Sazama, B. Wichterlova, The decisive role of the distribution of Al in the framework of beta zeolites on the structure and activity of Co ion species in propane-SCR-NOx in the presence of water vapour, J. Catal. 272 (2010) 44–54.

[7] N.V. Beznis, B.M. Weckhuysen, J.H. Bitter, Cu-ZSM-5 zeolites for the formation of methanol from methane and oxygen: probing the active sites and spectator species, Catal. Lett. 138 (2010) 14–22.

[8] A. Corma, A. Palomares, F. Marquez, Determining the nature of the active sites of Cu-beta zeolites for the selective catalytic reduction (SCR) of NOx by using a coupled reaction XAES/XPS study, J. Catal. 170 (1997) 132–139.

[9] H.Y. Chen, W.M.H. Sachtler, Activity and durability of Fe/ZSM-5 catalysts for lean burn NOx reduction in the presence of water vapor, Catal. Today 42 (1998) 73–83.

[10] R.Q. Long, R.T. Yang, Catalytic performance of Fe-ZSM-5 catalysts for selective catalytic reduction of nitric oxide by ammonia, J. Catal. 188 (1999) 332–339.

[11] M.S. Kumar, M. Schwidder, W. Grunert, A. Bruckner, On the nature of different iron sites and their catalytic role in Fe-ZSM-5 DeNO(x) catalysts: new insights by a combined EPR and UV/VIS spectroscopic approach, J. Catal. 227 (2004) 384–397.

[12] T. Tabata, H. Ohtsuka, L.M.F. Sabatino, G. Bellussi, Selective catalytic reduction of NOx by propane on Co-loaded zeolites, Microporous Mesoporous Mater. 21 (1998) 517–524.

[13] M.H. Groothaert, P.J. Smeets, B.F. Sels, P.A. Jacobs, R.A. Schoonheydt, Selective oxidation of methane by the bis(μ-oxo) dicopper core stabilized on ZSM-5 and mordenite zeolites, J. Amer. Chem. Soc. 127 (2005) 1394–1395.

[14] R.B. Borade, A. Clearfield, Preparation of aluminum-rich beta zeolite, Microporous Mater. 5 (1996) 289–297.

[15] R.B. Borade, A. Clearfield, Synthesis of beta zeolite with high levels of tetrahedral aluminium, Chem. Commun. (1996) 625–626.

[16] B. Xie, J. Song, L. Ren, Y. Ji, J. Li, F.S. Xiao, Organotemplate-free and fast route for synthesizing beta zeolite, Chem. Mater. 20 (2008) 4533–4535.

[17] K. Shanjiao, D. Tao, L. Qiang, D. Aijun, Z. Yanying, P. Huifang, Preparation and application of zeolite beta with super-low SiO$_2$/Al$_2$O$_3$ ratio, J. Porous Mater. 15 (2008) 159–162.

[18] G. Majano, L. Delmotte, V. Valtchev, S. Mintova, Al-rich zeolite beta by seeding in the absence of organic template, Chem. Mater. 21 (2009) 4184–4191.

[19] Y. Kamimura, W. Chaikittisilp, K. Itabashi, A. Shimojima, T. Okubo, Critical factors in the seed-assisted synthesis of zeolite beta and green beta from OSDA-Free Na$^+$-aluminosilicate gels, Chem. Asian J. 5 (2010) 2182–2191.

[20] Y. Kamimura, S. Tanahashi, K. Itabashi, A. Sugawara, T. Wakihara, A. Shimojima, T. Okubo, Crystallization behavior of zeolite beta in OSDA-free, seed-assisted synthesis, J. Phys. Chem. C 115 (2011) 744–750.

[21] B. Xie, H. Zhang, C. Yang, S. Liu, L. Ren, L. Zhang, X. Meng, B. Yilmaz, U. Muller, F.-S. Xiao, Seed-directed synthesis of zeolites with enhanced performance in the absence of organic templates, Chem. Commun. 47 (2011) 3945–3947.

[22] K. Itabashi, Y. Kamimura, K. Iyoki, A. Shimojima, T. Okubo, A working hypothesis for broadening framework types of zeolites in seed-assisted synthesis without organic structure-directing agent, J. Amer. Chem. Soc. 134 (2012) 11542–11549.

[23] B. Yilmaz, U. Muller, M. Feyen, H. Zhang, X. Meng, F.S. Xiao, X. Bao, W. Zhang, H. Imai, T. Yokoi, T. Tatsumi, H. Gies, T. De Baerdemaeker, D. De Vos, A new catalyst platform: zeolite beta from template-free synthesis, Catal. Sci. Technol. 3 (2013) 2580–2586.

[24] T. De Baerdemaeker, B. Yilmaz, U. Muller, M. Feyen, F.S. Xiao, W. Zhang, T. Tatsumi, H. Gies, X. Bao, D. De Vos, Catalytic applications of OSDA-free beta zeolite, J. Catal. 308 (2013) 73–81.

[25] H. Zhang, B. Xie, X. Meng, U. Mueller, B. Yilmaz, M. Feyen, S. Maurer, H. Gies, T. Tatsumi, X. Bao, W. Zhang, D. De Vos, F.-S. Xiao, Rational synthesis of Beta zeolite with improved quality by decreasing crystallization temperature in organotemplate-free route, Microporous Mesoporous Mater. 180 (2013) 123–129.

[26] Y. Kubota, K. Itabashi, S. Inagaki, Y. Nishita, R. Komatsu, Y. Tsuboi, S. Shinoda, T. Okubo, Effective fabrication of catalysts from large-pore, multidimensional zeolites synthesized without using organic structure-directing agents, Chem. Mater. 26 (2014) 1250–1259.

[27] B. Zheng, Y. Wan, W. Yang, F. Ling, H. Xie, X. Fang, H. Guo, Mechanism of seeding in hydrothermal synthesis of zeolite beta with organic structure-directing agent-free gel, Chin. J. Catal. 35 (2014) 1800–1810.

[28] P. Sazama, B. Wichterlova, S. Sklenak, V.I. Parvulescu, N. Candu, G. Sadovska, J. Dedecek, P. Klein, V. Pashkova, P. Stastny, Acid and redox activity of template-free Al-rich H-BEA* and Fe-BEA* zeolites, J. Catal. 318 (2014) 22–33.

[29] P. Sazama, L. Mokrzycki, B. Wichterlova, A. Vondrova, R. Pilar, J. Dedecek, S. Sklenak, E. Tabor, Unprecedented propane-SCR-NOx activity over template-free synthesized Al-rich Co-BEA* zeolite, J. Catal. 332 (2015) 201–211.

[30] P. Sazama, E. Tabor, P. Klein, B. Wichterlova, S. Sklenak, L. Mokrzycki, V. Pashkkova, M. Ogura, J. Dedecek, Al-rich beta zeolites. Distribution of Al atoms in the framework and related protonic and metal-ion species, J. Catal. 333 (2016) 102–114.

[31] P. Sazama, B. Wichterlova, E. Tabor, P. Stastny, N.K. Sathu, Z. Sobalik, J. Dedecek, S. Sklenak, P. Klein, A. Vondrova, Tailoring of the structure of Fe-cationic species in Fe-ZSM-5 by distribution of Al atoms in the framework for N$_2$O decomposition and NH$_3$-SCR-NOx, J. Catal. 312 (2014) 123–138.

[32] S. Brandenberger, O. Kröcher, A. Tissler, R. Althoff, The determination of the activities of different iron species in Fe-ZSM-5 for SCR of NO by NH$_3$, Appl. Catal. B: Environ. 95 (2010) 348–357.

[33] H.Y. Huang, R.Q. Long, R.T. Yang, Kinetics of selective catalytic reduction of NO with NH$_3$ on Fe-ZSM-5 catalyst, Appl. Cata. A: Gen. 235 (2002) 241–251.

[34] S. Civis, D. Babankova, J. Cihelka, P. Sazama, L. Juha, Spectroscopic investigations of high-power laser-induced dielectric breakdown in gas mixtures containing carbon monoxide, J. Phys. Chem. A 112 (2008) 7162–7169.

[35] A. Corma, V. Fornes, E. Palomares, Selective catalytic reduction of NOx on Cu-beta zeolites, Appl. Catal. B: Environ. 11 (1997) 233–242.

[36] M. Iwamoto, H. Hamada, Removal of nitrogen monoxide from exhaust gases through novel catalytic processes, Catal. Today 10 (1991) 57–71.

[37] G. Delahay, B. Coq, L. Broussous, Selective catalytic reduction of nitrogen monoxide by decane on copper-exchanged beta zeolites, Appl. Catal. B: Environ. 12 (1997) 49–59.

[38] R. Hierl, H. Knözinger, H.P. Urbach, Surface properties and reduction behavior of calcined CuO Al$_2$O$_3$ and CuO-NiO Al$_2$O$_3$ catalysts, J. Catal. 69 (1981) 475–486.

[39] J. Dĕdeček, O. Bortnovsky, A. Vondrová, B. Wichterlová, Catalytic activity of Cu-beta zeolite in NO decomposition: effect of copper and aluminium distribution, J. Catal. 200 (2001) 160–170.

[40] H. Praliaud, S. Mikhailenko, Z. Chajar, M. Primet, Surface and bulk properties of Cu–ZSM-5 and Cu/Al$_2$O$_3$ solids during redox treatments. Correlation with the selective reduction of nitric oxide by hydrocarbons, Appl. Catal. B: Environ. 16 (1998) 359–374.

[41] Z. Sobalik, P. Sazama, J. Dedecek, B. Wichterlova, Critical evaluation of the role of the distribution of Al atoms in the framework for the activity of metallo-zeolites in redox N$_2$O/NOx reactions, Appl. Cata. A: Gen. 474 (2014) 178–185.

[42] J. Dedecek, L. Capek, P. Sazama, Z. Sobalik, B. Wichterlova, Control of metal ion species in zeolites by distribution of aluminium in the framework: from structural analysis to performance under real conditions of SCR-NOx and NO N$_2$O decomposition, Appl. Cata. A: Gen. 391 (2011) 244–253.

[43] L. Xu, C. Shi, Z. Zhang, H. Gies, F.-S. Xiao, D. De Vos, T. Yokoi, X. Bao, M. Feyen, S. Maurer, U. Mueller, W. Zhang, Enhancement of low-temperature activity over Cu-exchanged zeolite beta from organotemplate-free synthesis for the selective catalytic reduction of NO with NH$_3$ in exhaust gas streams, Microporous Mesoporous Mater. 200 (2014) 304–310.

[44] S.T. Korhonen, D.W. Fickel, R.F. Lobo, B.M. Weckhuysen, A.M. Beale, Isolated Cu^{2+} ions: active sites for selective catalytic reduction of NO, Chem. Commun. 47 (2011) 800–802.

[45] G. Delahay, B. Coq, S. Kieger, B. Neveu, The origin of N$_2$O formation in the selective catalytic reduction of NOx by NH$_3$ in O$_2$ rich atmosphere on Cu-faujasite catalysts, Catal. Today 54 (1999) 431–438.

[46] P. Sazama, O. Bortnovsky, J. Dedecek, Z. Tvaruzkova, Z. Sobalik, Geopolymer based catalysts-new group of catalytic materials, Catal. Today 164 (2011) 92–99.

[47] G.D. Pirngruber, P.K. Roy, R. Prins, On determining the nuclearity of iron sites in Fe-ZSM-5—a critical evaluation, Phys. Chem. Chem. Phys. 8 (2006) 3939–3950.

[48] L. Capek, V. Kreibich, J. Dedecek, T. Grygar, B. Wichterlova, Z. Sobalik, J.A. Martens, R. Brosius, V. Tokarova, Analysis of Fe species in zeolites by UV-VIS-NIR, IR spectra and voltammetry. Effect of preparation Fe loading and zeolite type, Microporous Mesoporous Mater. 80 (2005) 279–289.

[49] S. Bordiga, R. Buzzoni, F. Geobaldo, C. Lamberti, E. Giamello, A. Zecchina, G. Leofanti, G. Petrini, G. Tozzola, G. Vlaic, Structure and reactivity of framework and extraframework iron in Fe-silicalite as investigated by spectroscopic and physicochemical methods, J. Catal. 158 (1996) 486–501.

[50] H.Y. Chen, T. Voskoboinikov, W.M.H. Sachtler, Reduction of NOx over Fe/ZSM-5 catalysts: adsorption complexes and their reactivity toward hydrocarbons, J. Catal. 180 (1998) 171–183.

[51] X.B. Feng, W.K. Hall, FeZSM-5: a durable SCR catalyst for NOx removal from combustion streams, J. Catal. 166 (1997) 368–376.

[52] G. Fierro, G. Moretti, G. Ferraris, G.B. Andreozzi, A Mössbauer and structural investigation of Fe-ZSM-5 catalysts: influence of Fe oxide nanoparticles size on the catalytic behaviour for the NO-SCR by C_3H_8, Appl. Catal. B: Environ. 102 (2011) 215–223.

[53] L. Capek, J. Dedecek, B. Wichterlova, Co-beta zeolite highly active in propane-SCR-NOx in the presence of water vapor: effect of zeolite preparation and A1 distribution in the framework, J. Catal. 227 (2004) 352–366.

[54] J. Dedecek, L. Capek, D. Kaucky, Z. Sobalik, B. Wichterlova, Siting and distribution of the Co ions in beta zeolite: a UV–Vis–NIR and FTIR study, J. Catal. 211 (2002) 198–207.

[55] D. Barreca, C. Massignan, S. Daolio, M. Fabrizio, C. Piccirillo, L. Armelao, E. Tondello, Composition and microstructure of cobalt oxide thin films obtained from a novel cobalt(II) precursor by chemical vapor deposition, Chem. Mater. 13 (2001) 588–593.

[56] V.M. Jimenez, A. Fernandez, J.P. Espinos, A.R. Gonzalezelipe, The state of the oxygen at the surface of polycrystalline cobalt oxide, J. Electron Spectrosc. Relat. Phenom. 71 (1995) 61–71.

[57] A.Y. Khodakov, A. Griboval-Constant, R. Bechara, V.L. Zholobenko, Pore size effects in Fischer Tropsch synthesis over cobalt-supported mesoporous silicas, J. Catal. 206 (2002) 230–241.

[58] H.H. Chen, S.C. Shen, X. Chen, S. Kawi, Selective catalytic reduction of NO over Co/beta-zeolite: effects of synthesis condition of beta-zeolites, Co precursor, Co loading method and reductant, Appl. Catal. B: Environ. 50 (2004) 37–47.

[59] X.Y. Chen, S.C. Shen, H.H. Chen, S. Kawi, SCR of lean NOx with C_3H_8 over Co/MFI catalysts: dependence on synthesis condition of MFI and Co location, J. Catal. 221 (2004) 137–147.